arXiv:1701.01233v1 [math.NA] 5 Jan 2017

A Meshing Strategy for a Quadratic Iso-parametric FEM in Cavitation Computation in Nonlinear Elasticity*

Chunmei Su and Zhiping Li†

LMAM & School of Mathematical Sciences,

Peking University, Beijing 100871, China

Abstract

The approximation properties of a quadratic iso-parametric finite element method for a typical cavitation problem in nonlinear elasticity are analyzed. More precisely, (1) the finite element interpolation errors are established in terms of the mesh parameters; (2) a mesh distribution strategy based on an error equi-distribution principle is given; (3) the convergence of finite element cavity solutions is proved. Numerical experiments show that, in fact, the optimal convergence rate can be achieved by the numerical cavity solutions.

Keywords: cavitation, quadratic iso-parametric FEM, error analysis, meshing strategy, convergence, nonlinear elasticity.

AMS Subject Classification: 65N12, 65N15, 65N30, 65N50, 74B20, 74G15,74M99.

*The research was supported by the NSFC project 11171008 and RFDP of China.

†Corresponding author, email: lizp@math.pku.edu.cn

1 Introduction

Nonlinear soft elastic materials, such as polymers, biological tissues, rubbers, etc., can display a particular singular deformation, referred to in the literature as cavitation, when strong external force is applied [6, 7, 9, 17, 25]. The occurrence and growth of cavities is considered closely related to the material instability and to the damage and failure mechanisms of the materials [10, 14, 15, 16, 19]. A huge number of work has been done by numerous authors analysing cavitation experimentally, theoretically as well as numerically.

Generally speaking, there are two representative approaches characterizing cavitation. One is the so-called defect model, which is based on the hypothesis that cavities grow from pre-existing micro defects. Under this assumption, Gent and Lindley [9] analysed the critical hydrostatic pressure at which a given unit spherical void in an infinite extension of a Neo-Hookean material would blow up, which was in a good agreement with their experiments therein. The other is the perfect model established by Ball [3] based on the analytical evidence that, under certain circumstances, a deformation with cavities created in an originally intact material can be energetically favorable. It is shown that, under the assumption that the cavities can appear only at a finite number of fixed points in the intact materials, the solution of the defect model converges to the solution of the perfect model [11, 32] as the radii of the pre-existing small voids go to zero. In addition, analytical and numerical evidences indicate that whether a point can serve as a possible position of cavitation can be evaluated by calculating the corresponding configurational forces [22, 31].

The perfect model typically exhibits the Lavrentiev phenomenon [18] when there is a cavitation solution, leading to the failure of the conventional finite element methods [1, 4]. Though there are existing numerical methods developed to deal with the Lavrentiev phenomenon [1, 4, 20, 28], they do not seem to be suitable to tackle the cavitation problem. In fact, most of the numerical studies on cavitation are based on the defect model, in which one considers to minimize

the total energy of the form

$$E(\boldsymbol{u}) = \int_{\Omega_\varrho} W(\nabla \boldsymbol{u}(\boldsymbol{x}))d\boldsymbol{x}, \tag{1.1}$$

in the set of admissible functions

$$\mathcal{A} = \{\boldsymbol{u} \in W^{1,p}(\Omega_\varrho;\mathbb{R}^n) \text{ is one-to-one a.e. : } \boldsymbol{u}|_{\Gamma_0} = \boldsymbol{u}_0, \det \nabla \boldsymbol{u} > 0 \ a.e.\}, \tag{1.2}$$

where $\Omega_\varrho = \Omega \setminus \bigcup_{i=1}^m B_{\varrho_i}(\boldsymbol{a}_i) \subset \mathbb{R}^n \, (n = 2, 3)$ denotes the region occupied by an elastic body in its reference configuration, $B_{\varrho_i}(\boldsymbol{a}_i) = \{\boldsymbol{x} \in \mathbb{R}^n : |\boldsymbol{x} - \boldsymbol{a}_i| < \varrho_i\}$ is the pre-existing spherical hole centered at $\boldsymbol{a}_i$ with small radius $\varrho_i > 0$, $W : M_+^{n\times n} \to \mathbb{R}^+$ is the elastic stored energy density of the material, $M_+^{n\times n}$ denotes the set of $n \times n$ matrices with positive determinant, Γ_0 is the boundary of Ω.

A typical example of the elastic stored energy density is of the form

$$W(F) = \omega|F|^p + g(\det F), \quad \forall F \in M_+^{n\times n}, \tag{1.3}$$

where $\omega > 0$ is a material constant, $n - 1 < p < n$, and $g : (0, \infty) \to (0, \infty)$ is a continuously differentiable strictly convex function characterizing the compressibility of the material and satisfies

$$g(d) \to +\infty \text{ as } d \to 0, \text{ and } \frac{g(d)}{d} \to +\infty \text{ as } d \to +\infty. \tag{1.4}$$

As was shown by Ball [3], this kind of functional can have a singular minimizer displaying cavitation. Further studies on the existence of singular minimizers in Sobolev spaces are referred to [11, 27, 30].

One of the main difficulties in the computation of immense growth of voids is the orientation-preservation of the finite element deformation, which is a crucial constraint and is characterized by the pointwise positivity of the Jacobian determinant of the deformation gradient. For the conforming piecewise affine finite element, the condition leads to an unbearably large amount of degrees of freedom [35]. Some numerical methods [21, 22, 23, 35] have been designed to overcome the difficulty, and have shown some success numerically. However, strict analytical results are insufficient. The only practical analytical results for

the cavitation computation known to the authors so far are [34], where a sufficient orientation-preservation condition and the interpolation error estimates were given for a dual-parametric bi-quadratic finite element method, and [33], where a set of sufficient and necessary orientation-preservation conditions for the quadratic iso-parametric finite element interpolation functions of radially symmetric cavity deformations are derived.

In this paper, we analyze the approximation properties of a quadratic iso-parametric finite element for the typical cavitation problem. The analytical results on the errors of finite element interpolation functions lead to a delicate relationship between the elastic energy error and the mesh parameters, which together with the orientation-preservation conditions (see Remark 3.4 and [33]) enable us to establish a mesh distribution strategy guaranteeing that the corresponding finite element cavitation solution is orientation preserving and its relative error on the elastic energy is $O(h^2)$, where h is the mesh size in the far field, *i.e.* a given distance away from the cavity. Above all, for the first time to our knowledge, the convergence of the finite element cavitation solutions in $W^{1,p}$ norm is proved. In fact, the numerical experiments show that the optimal order of convergence rate is achieved by the numerical cavitation solutions obtained on the meshes produced by our meshing strategy.

Since the cavitation solution is generally considered to be quite regular except in a neighborhood of the voids, where the material experiences extremely large expansion dominant deformations and the difficulty of the computation as well as analysis lies, we restrict ourselves to a simplified problem with $\Omega_\varrho = B_1(\mathbf{0}) \setminus B_\varrho(\mathbf{0})$ in $\mathbb{R}^2$ and a simple expansionary boundary condition given by $\boldsymbol{u}_0 = \lambda \boldsymbol{x}$.

The structure of the paper is as follows. In § 2, we introduce the iso-parametric finite element method and a radially symmetric large expansion accommodating triangulation method briefly. § 3 is devoted to analyzing the interpolation errors of the cavitation solutions. The meshing strategy is given in § 4, where the convergence theorem is also established. The numerical results are presented in § 5. Some concluding remarks are made in § 6.

2 Preliminaries

2.1 The quadratic iso-parametric FEM

Let $(\hat{T}, \hat{P}, \hat{\Sigma})$ be a quadratic Lagrange reference element. Define $F_T : \hat{T} \to \mathbb{R}^2$

$$\begin{cases} F_T \in \hat{P}^2 = (P_2(\hat{T}))^2, \\ \boldsymbol{x} = F_T(\hat{\boldsymbol{x}}) = \sum_{i=1}^{3} \boldsymbol{a}_i \hat{\mu}_i(\hat{\boldsymbol{x}}) + \sum_{1 \le i < j \le 3} \boldsymbol{a}_{ij} \hat{\mu}_{ij}(\hat{\boldsymbol{x}}), \end{cases} \tag{2.1}$$

where $\boldsymbol{a}_i, 1 \le i \le 3$, and $\boldsymbol{a}_{ij}, 1 \le i < j \le 3$ are given points in $\mathbb{R}^2$, and

$$\hat{\mu}_i(\hat{\boldsymbol{x}}) = \hat{\lambda}_i(\hat{\boldsymbol{x}})(2\hat{\lambda}_i(\hat{\boldsymbol{x}}) - 1), \quad \hat{\mu}_{ij}(\hat{\boldsymbol{x}}) = 4\hat{\lambda}_i(\hat{\boldsymbol{x}})\hat{\lambda}_j(\hat{\boldsymbol{x}}),$$

with $\hat{\lambda}_i(\hat{\boldsymbol{x}}), 1 \le i \le 3$ being the barycentric coordinates of $\hat{T}$. If the map F_T defined above is an injection, then, $T = F_T(\hat{T})$ is a curved triangular element as shown in Figure 2. The standard quadratic iso-parametric finite element is defined as a finite element triple (T, P_T, Σ_T) with

$$\begin{cases} T = F_T(\hat{T}) \text{ being a curved triangle element}, \\ P_T = \{p : T \to \mathbb{R} \mid p = \hat{p} \circ F_T^{-1},\ \hat{p} \in \hat{P} = P_2(\hat{T})\}, \\ \Sigma_T = \{p(\boldsymbol{a}_i), 1 \le i \le 3; p(\boldsymbol{a}_{ij}), 1 \le i < j \le 3\}. \end{cases} \tag{2.2}$$

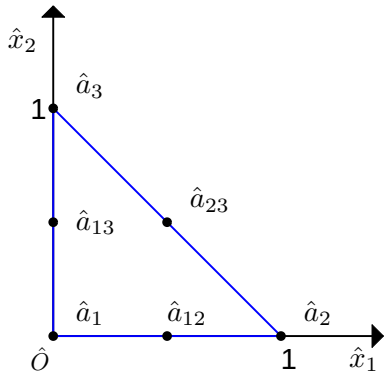

Figure 1: The reference element $\hat{T}$.

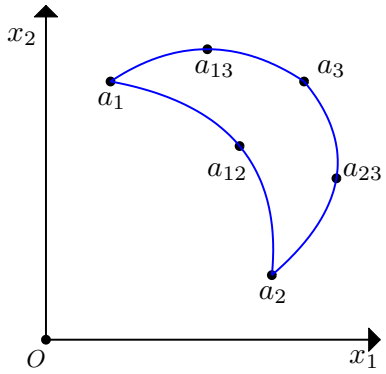

Figure 2: A curved triangular element T.

2.2 Large expansion accommodating triangulations

Let's have a look at how the iso-parametric FEM is applied in cavitation computation. As introduced in [22], let $\boldsymbol{x}_k$ $(k = 1, \cdots, m)$ be the center of the $k-$th defect with small radius ϱ_k. In the domain far away from the defects where the deformation is regular, the mesh is given by general straight edged triangulation. To accommodate the large expansionary deformation around the defects, the triangulation near the defects is given by the quadratic mapping as in (2.1), where given 3 vertices $\boldsymbol{a}_i$, denote $(r_k(\boldsymbol{x}), \theta_k(\boldsymbol{x}))$ the local polar coordinates of $\boldsymbol{x}$ with respect to $\boldsymbol{x}_k$, set

$$\boldsymbol{a}_{ij} = (r_{ij}\cos\theta_{ij}, r_{ij}\sin\theta_{ij}) + \boldsymbol{x}_k, \tag{2.3}$$

where

$$r_{ij} = \frac{r(\boldsymbol{a}_i) + r(\boldsymbol{a}_j)}{2}, \quad \theta_{ij} = \frac{\theta(\boldsymbol{a}_i) + \theta(\boldsymbol{a}_j)}{2}.$$

Moreover, the elements on the boundary are also adjusted to achieve a better approximation of the region. With this kind of curved elements near the defects and general straight triangles elsewhere, the mesh can better accommodate the locally large expansionary deformations. As an example, an EasyMesh produced mesh $\mathcal{J}'$ with $m = 2$ is shown in Figure 3, and the final mesh $\mathcal{J}$ (see Figure 4) is obtained by adding to $\mathcal{J}'$ around each defect two layers of radially symmetric mesh of the kind shown in Figure 5(a), which is a standard curved triangulation around a prescribed circular ring with inner radius $\epsilon = 0.01$ and thickness $\tau = 0.01$. Figure 5(b) shows that an outer layer of standard curved triangulation is connected to a doubly refined inner one by a conforming layer of nonstandard curved triangulation. For the convenience of reference, we classify the curved triangular elements in Figure 5 into four basic types, and denote them as types A, B, C and D.

3 Interpolation errors of cavity deformations

There are standard error estimates [5] on the interpolation functions in the iso-parametric finite element function spaces, however, because of the highly

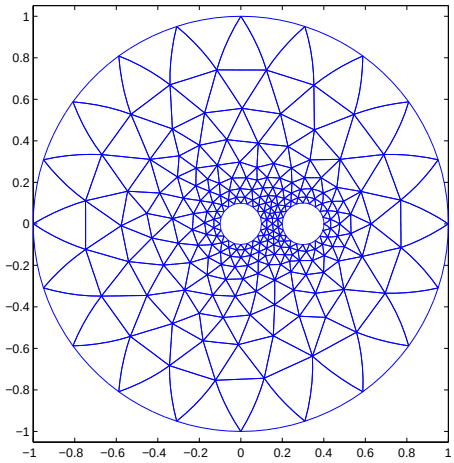

Figure 3: An EasyMesh $\mathcal{J}'$.

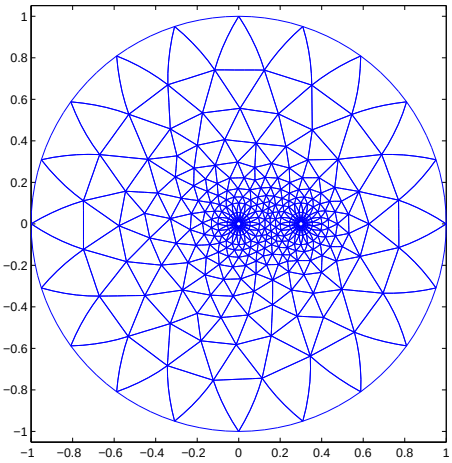

Figure 4: $\mathcal{J}$, a mesh adapted to cavity.

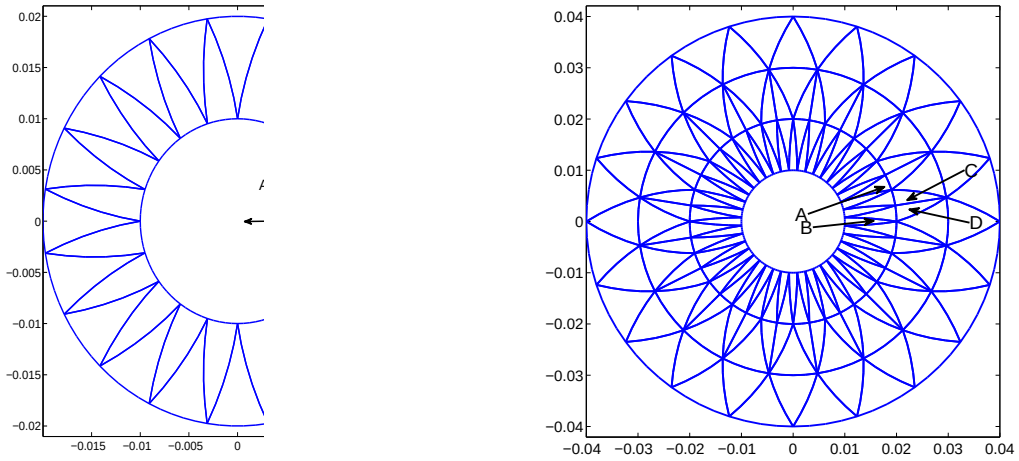

(a) A standard layer of curved triangulation. (b) A conforming layer links 2 standard ones.

Figure 5: Triangulation layers with elements of types A, B, C and D.

anisotropic deformation inevitably involved in the cavitation computation, the error bounds so obtained depend generally on the size of the initial void ϵ_0 and blow up when $\epsilon_0 \to 0$. In this section, with some more sophisticated manipulations and calculations, we are able to establish the ϵ_0-independent interpolation error estimates, including those on the deformation and its Jacobian determinant, and in particular the elastic energy, for the radially symmetric cavity deforma-

tions in the quadratic iso-parametric finite element function spaces defined on the meshes consisting of only elements of types A, B, C and D.

To have a better picture in our mind for the problem given below, we first introduce some notations. Let ϵ and τ represent respectively the inner radius and the thickness of the circular annulus as shown in Figure 5(a), let N be the number of the evenly spaced nodes on the outer circle of the circular ring, and denote $\Omega_{(\epsilon,\tau)} = \{\boldsymbol{x} \in \mathbb{R}^2 : \epsilon \le |\boldsymbol{x}| \le \epsilon + \tau\}$. Throughout the paper, the notation $\Phi \lesssim \Psi$ means that there exists a generic constant C independent of ϵ and τ such that $|\Phi| \le C\Psi$, and $\Phi \sim \Psi$ means that $\Psi \lesssim \Phi \lesssim \Psi$.

3.1 The interpolation function and its Jacobian

For a radially symmetric function $\boldsymbol{v}(\boldsymbol{x}) = \frac{s(|\boldsymbol{x}|)}{|\boldsymbol{x}|}\boldsymbol{x}$, the iso-parametric finite element interpolation function can be written as (see § 2)

$$\Pi\boldsymbol{v}(\boldsymbol{x}) = \sum_{i=1}^{3} \boldsymbol{b}_i \hat{\mu}_i(\hat{\boldsymbol{x}}) + \sum_{1\le i<j\le 3} \boldsymbol{b}_{ij}\hat{\mu}_{ij}(\hat{\boldsymbol{x}}), \tag{3.1}$$

where $\hat{\boldsymbol{x}} = F_T^{-1}(\boldsymbol{x})$, and where, for a representative of type A element, $\boldsymbol{b}_1 = (s_0, 0)$, $\boldsymbol{b}_2 = s_1(\cos\frac{\pi}{N}, -\sin\frac{\pi}{N})$, $\boldsymbol{b}_3 = s_1(\cos\frac{\pi}{N}, \sin\frac{\pi}{N})$, $\boldsymbol{b}_{12} = s_{1/2}(\cos\frac{\pi}{2N}, -\sin\frac{\pi}{2N})$, $\boldsymbol{b}_{13} = s_{1/2}(\cos\frac{\pi}{2N}, \sin\frac{\pi}{2N})$, $\boldsymbol{b}_{23} = (s_1, 0)$. On this element, let $y = \hat{x}_1 + \hat{x}_2$ and $z = \hat{x}_1\hat{x}_2$, we have

$$\Pi\boldsymbol{v}(\boldsymbol{x}) = \left(s_0 + \alpha_2 y + 2\alpha_1 y^2 - 4s_1 \sin^2\frac{\pi}{2N}(\hat{x}_1^2 + \hat{x}_2^2), (2\gamma y - \beta)(\hat{x}_2 - \hat{x}_1)\right), \tag{3.2}$$

where

$$\alpha_1 = s_0 + s_1 - 2s_{1/2}\cos\frac{\pi}{2N}, \tag{3.3}$$

$$\alpha_2 = -3s_0 - s_1\cos\frac{\pi}{N} + 4s_{1/2}\cos\frac{\pi}{2N}, \tag{3.4}$$

$$\beta = s_1\sin\frac{\pi}{N} - 4s_{1/2}\sin\frac{\pi}{2N}, \tag{3.5}$$

$$\gamma = s_1\sin\frac{\pi}{N} - 2s_{1/2}\sin\frac{\pi}{2N}. \tag{3.6}$$

Hence

$$\frac{\partial \Pi \boldsymbol{v}}{\partial \hat{\boldsymbol{x}}} = \begin{pmatrix} \alpha - 8s_1\hat{x}_1 \sin^2 \frac{\pi}{2N} & \alpha - 8s_1\hat{x}_2 \sin^2 \frac{\pi}{2N} \\ \beta - 4\gamma\hat{x}_1 & -\beta + 4\gamma\hat{x}_2 \end{pmatrix}, \tag{3.7}$$

where $\alpha = 4\alpha_1 y + \alpha_2$. It follows that

$$\begin{aligned} \det \frac{\partial \Pi \boldsymbol{v}}{\partial \hat{\boldsymbol{x}}}(\hat{x}_1, \hat{x}_2) = H(y,z) \triangleq 16\gamma\alpha_1 y^2 - 64 s_1 \gamma \sin^2 \frac{\pi}{2N} z \\ + \big(-8\beta\big(\alpha_1 - s_1 \sin^2 \frac{\pi}{2N}\big) + 4\gamma\alpha_2\big) y - 2\beta\alpha_2. \end{aligned} \tag{3.8}$$

On a representative element of type B with $\boldsymbol{b}_1 = (s_1, 0)$, $\boldsymbol{b}_2 = s_0(\cos\frac{\pi}{N}, \sin\frac{\pi}{N})$, $\boldsymbol{b}_3 = s_0(\cos\frac{\pi}{N}, -\sin\frac{\pi}{N})$, $\boldsymbol{b}_{12} = s_{1/2}(\cos\frac{\pi}{2N}, \sin\frac{\pi}{2N})$, $\boldsymbol{b}_{13} = s_{1/2}(\cos\frac{\pi}{2N}, -\sin\frac{\pi}{2N})$, $\boldsymbol{b}_{23} = (s_0, 0)$, again denote $y = \hat{x}_1 + \hat{x}_2$ and $z = \hat{x}_1\hat{x}_2$, one has

$$\Pi \boldsymbol{v}(\boldsymbol{x}) = \Big(s_1 + \bar{\alpha}_2 y + 2\bar{\alpha}_1 y^2 - 4 s_0 \sin^2 \frac{\pi}{2N}(\hat{x}_1^2 + \hat{x}_2^2), (2\bar{\gamma} y - \bar{\beta})(\hat{x}_1 - \hat{x}_2) \Big), \tag{3.9}$$

where

$$\bar{\alpha}_1 = s_0 + s_1 - 2s_{1/2} \cos \frac{\pi}{2N}, \tag{3.10}$$

$$\bar{\alpha}_2 = -3s_1 - s_0 \cos \frac{\pi}{N} + 4 s_{1/2} \cos \frac{\pi}{2N}, \tag{3.11}$$

$$\bar{\beta} = s_0 \sin \frac{\pi}{N} - 4 s_{1/2} \sin \frac{\pi}{2N}, \tag{3.12}$$

$$\bar{\gamma} = s_0 \sin \frac{\pi}{N} - 2 s_{1/2} \sin \frac{\pi}{2N}. \tag{3.13}$$

Hence

$$\frac{\partial \Pi \boldsymbol{v}}{\partial \hat{\boldsymbol{x}}} = \begin{pmatrix} \bar{\alpha} - 8s_0\hat{x}_1 \sin^2 \frac{\pi}{2N} & \bar{\alpha} - 8s_0\hat{x}_2 \sin^2 \frac{\pi}{2N} \\ -\bar{\beta} + 4\bar{\gamma}\hat{x}_1 & \bar{\beta} - 4\bar{\gamma}\hat{x}_2 \end{pmatrix}, \tag{3.14}$$

$$\begin{aligned} \det \frac{\partial \Pi \boldsymbol{v}}{\partial \hat{\boldsymbol{x}}} = H(y,z) = -16\bar{\gamma}\bar{\alpha}_1 y^2 + 64 s_0 \bar{\gamma} \sin^2 \frac{\pi}{2N} z \\ + (8\bar{\beta}(\bar{\alpha}_1 - s_0 \sin^2 \frac{\pi}{2N}) - 4\bar{\gamma}\bar{\alpha}_2) y + 2\bar{\beta}\bar{\alpha}_2. \end{aligned} \tag{3.15}$$

On a representative element of type C with $\boldsymbol{b}_1 = (s_0, 0)$, $\boldsymbol{b}_2 = (s_1, 0)$, $\boldsymbol{b}_3 = s_0(\cos\frac{\pi}{N}, \sin\frac{\pi}{N})$, $\boldsymbol{b}_{12} = (s_{1/2}, 0)$, $\boldsymbol{b}_{13} = s_0(\cos\frac{\pi}{2N}, \sin\frac{\pi}{2N})$, $\boldsymbol{b}_{23} = s_{1/2}(\cos\frac{\pi}{2N}, \sin\frac{\pi}{2N})$,

one has

$$\Pi\boldsymbol{v}(\boldsymbol{x}) = \Big(s_0+\tilde{\alpha}_1\hat{x}_1+s_0\tilde{\alpha}_2\hat{x}_2+2\tilde{\alpha}_3\hat{x}_1^2-8\sin^2\frac{\pi}{4N}\hat{x}_2\big(s_0\cos\frac{\pi}{2N}\hat{x}_2-(s_0-s_{1/2})\hat{x}_1\big),$$
$$2\sin\frac{\pi}{2N}\hat{x}_2\big(s_0(2-\cos\frac{\pi}{2N})-4s_0\sin^2\frac{\pi}{4N}\hat{x}_2+2(s_{1/2}-s_0)\hat{x}_1\big)\Big), \quad (3.16)$$

where $\tilde{\alpha}_1 = 4s_{1/2} - s_1 - 3s_0$, $\tilde{\alpha}_2 = 4\cos\frac{\pi}{2N} - \cos\frac{\pi}{N} - 3$, $\tilde{\alpha}_3 = s_0 + s_1 - 2s_{1/2}$.

Similarly, on a representative element of type D with $\boldsymbol{b}_1 = (s_0, 0)$, $\boldsymbol{b}_2 = s_0(\cos\frac{\pi}{N}, -\sin\frac{\pi}{N})$, $\boldsymbol{b}_3 = (s_1, 0)$, $\boldsymbol{b}_{12} = s_0(\cos\frac{\pi}{2N}, -\sin\frac{\pi}{2N})$, $\boldsymbol{b}_{13} = (s_{1/2}, 0)$, $\boldsymbol{b}_{23} = s_{1/2}(\cos\frac{\pi}{2N}, -\sin\frac{\pi}{2N})$, one has

$$\Pi\boldsymbol{v}(\boldsymbol{x}) = \Big(s_0+s_0\tilde{\alpha}_2\hat{x}_1+\tilde{\alpha}_1\hat{x}_2+2\tilde{\alpha}_3\hat{x}_2^2-8\sin^2\frac{\pi}{4N}\hat{x}_1\big(s_0\cos\frac{\pi}{2N}\hat{x}_1-(s_0-s_{1/2})\hat{x}_2\big),$$
$$-2\sin\frac{\pi}{2N}\hat{x}_1\big(s_0(2-\cos\frac{\pi}{2N})-4s_0\sin^2\frac{\pi}{4N}\hat{x}_1+2(s_{1/2}-s_0)\hat{x}_2\big)\Big). \quad (3.17)$$

Throughout this section, we assume that $\boldsymbol{u}(\boldsymbol{x}) = \frac{r(|\boldsymbol{x}|)}{|\boldsymbol{x}|}\boldsymbol{x}$ represent a cavity deformation, where $r(R)$ defined on $(0,1]$ is smooth, positive, increasing, and convex with $r^{(j)}(R)(j = 0, 1, 2, 3)$ bounded. Moreover, it satisfies $\inf_{R\in(0,1]} r(R) > 0$, $mR \le r'(R) \le MR$, with $0 < m < M$ which is shown to be naturally satisfied for the energy minimizer of (1.3) in [33]. For simplicity of the notations, we denote $y = \hat{x}_1 + \hat{x}_2 \in [0, 1]$, $z = \hat{x}_1\hat{x}_2 \in [0, \frac{y^2}{4}]$, where $\hat{\boldsymbol{x}} = (\hat{x}_1, \hat{x}_2) \in \hat{T}$.

3.2 The error of the interpolation function

We will estimate, in this subsection, the errors between $\boldsymbol{u}(\boldsymbol{x}) = \frac{r(|\boldsymbol{x}|)}{|\boldsymbol{x}|}\boldsymbol{x}$ and its interpolation function $\Pi\boldsymbol{u}(\boldsymbol{x})$ in the polar coordinates. Let (R, θ) be the polar coordinates of $\boldsymbol{x}$ on the reference configuration and let (ζ, φ) be the polar coordinates of the interpolation function $\Pi\boldsymbol{u}(\boldsymbol{x})$ of $\boldsymbol{u}(\boldsymbol{x}) = \frac{r(|\boldsymbol{x}|)}{|\boldsymbol{x}|}\boldsymbol{x} = (r(R), \theta)$ on the deformed configuration.

Lemma 3.1 *Denote $\boldsymbol{x} = F_T(\hat{\boldsymbol{x}}) = R(\cos\theta, \sin\theta)$, then for the typical element A, one has*

$$R = \epsilon + \tau y + O(\tau N^{-2} + \epsilon N^{-4}) = (\epsilon + \tau y)(1 + O(N^{-2})), \quad (3.18)$$
$$\theta = \frac{\pi}{N}(\hat{x}_2 - \hat{x}_1) + O(N^{-3}), \quad (3.19)$$
$$\det\nabla\boldsymbol{x} = 4\tau\sin\frac{\pi}{2N}(\epsilon + \tau y + 2\tau\sin^2\frac{\pi}{4N})\big(1 + O(N^{-2} + \frac{\epsilon}{\tau}N^{-4})\big); \quad (3.20)$$

for the typical element B, we have

$$R = \epsilon + \tau(1-y) + O(\tau + \epsilon N^{-2})N^{-2} = (\epsilon + \tau(1-y))(1 + O(N^{-2})), \quad (3.21)$$

$$\theta = \frac{\pi}{N}(\hat{x}_1 - \hat{x}_2) + O(N^{-3}), \quad (3.22)$$

$$\det \nabla \boldsymbol{x} = 4\tau \sin\frac{\pi}{2N}\big(\epsilon + \tau(1-y)\big)\big(1 + O(N^{-2} + \frac{\epsilon}{\tau}N^{-4})\big); \quad (3.23)$$

for the typical element C, one has

$$\begin{aligned} R &= \epsilon + \tau\hat{x}_1 + O(\tau N^{-2} + \epsilon N^{-4}) = (\epsilon + \tau\hat{x}_1)(1 + O(N^{-2})), & (3.24)\\ \theta &= \frac{\pi}{N}\hat{x}_2 + O(N^{-3}), & (3.25)\\ \det \nabla \boldsymbol{x} &= 2\tau \sin\frac{\pi}{2N}(\epsilon + \tau\hat{x}_1)\big(1 + O(N^{-2})\big); & (3.26) \end{aligned}$$

while for the typical element D, one has

$$\begin{aligned} R &= \epsilon + \tau\hat{x}_2 + O(\tau N^{-2} + \epsilon N^{-4}) = (\epsilon + \tau\hat{x}_2)(1 + O(N^{-2})), & (3.27)\\ \theta &= -\frac{\pi}{N}\hat{x}_1 + O(N^{-3}), & (3.28)\\ \det \nabla \boldsymbol{x} &= 2\tau \sin\frac{\pi}{2N}(\epsilon + \tau\hat{x}_2)\big(1 + O(N^{-2})\big). & (3.29) \end{aligned}$$

Proof. For a typical type A element, it follows from (3.2) that $x_1 = t_1 + t_2 z, x_2 = t_3(\hat{x}_2 - \hat{x}_1)$, where

$$\begin{aligned} t_1 &= \epsilon + \hat{\alpha}_2 y + \hat{\alpha}_4 y^2, \qquad t_2 = 2\hat{\gamma}y - \hat{\beta}, \quad t_3 = 8(\epsilon+\tau)\sin^2\frac{\pi}{2N},\\ \hat{\alpha}_4 &= 2\epsilon + 2(\epsilon+\tau)\cos\frac{\pi}{N} - 4(\epsilon + \frac{\tau}{2})\cos\frac{\pi}{2N}\\ &= -2\epsilon\sin^2\frac{\pi}{2N} + O(\tau N^{-2} + \epsilon N^{-4}), & (3.30) \end{aligned}$$

$\hat{\alpha}_2$, $\hat{\beta}$, $\hat{\gamma}$ are given by (3.4)-(3.6) by taking $s(t) = t$, i.e.,

$$\begin{aligned} \hat{\alpha}_2 &= -3\epsilon + 4(\epsilon + \frac{\tau}{2})\cos\frac{\pi}{2N} - (\epsilon+\tau)\cos\frac{\pi}{N} = \tau + O(\tau N^{-2} + \epsilon N^{-4}), & (3.31)\\ \hat{\beta} &= (\epsilon+\tau)\sin\frac{\pi}{N} - 4(\epsilon + \frac{\tau}{2})\sin\frac{\pi}{2N}\\ &= -2\epsilon\sin\frac{\pi}{2N} - 4(\epsilon+\tau)\sin\frac{\pi}{2N}\sin^2\frac{\pi}{4N}, & (3.32)\\ \hat{\gamma} &= (\epsilon+\tau)\sin\frac{\pi}{N} - 2(\epsilon + \frac{\tau}{2})\sin\frac{\pi}{2N}\\ &= \tau\sin\frac{\pi}{2N} - 4(\epsilon+\tau)\sin\frac{\pi}{2N}\sin^2\frac{\pi}{4N}. & (3.33) \end{aligned}$$

Thus, by $0 \le y \le 1$, $\frac{y}{\epsilon+\tau y} \le \frac{1}{\epsilon+\tau}$, one has

$$\begin{aligned} x_1 &= \epsilon + \tau y - 2\epsilon \sin^2 \frac{\pi}{2N}(y^2 - 4z) + O(\tau + \epsilon N^{-2})N^{-2} y \\ &= (\epsilon + \tau y)(1 + O(N^{-2})), \\ x_2 &= 2 \sin \frac{\pi}{2N}(\epsilon + \tau y - 2(\epsilon + \tau) \sin^2 \frac{\pi}{4N}(2y - 1))(\hat{x}_2 - \hat{x}_1), \end{aligned}$$

hence

$$\begin{aligned} R^2 &= (\epsilon + \tau y)^2 - 4\epsilon(\epsilon + \tau y) \sin^2 \frac{\pi}{2N}(y^2 - 4z) + (\epsilon + \tau y) O(\epsilon N^{-4} + \tau N^{-2}) y \\ &\qquad + \tau^2 N^{-6} y^2 + 4(\epsilon + \tau y)^2 \sin^2 \frac{\pi}{2N}(y^2 - 4z) \\ &= (\epsilon + \tau y)^2 \Big(1 + \frac{O(\tau N^{-2} + \epsilon N^{-4}) y}{\epsilon + \tau y} + \frac{O(\tau^2 N^{-6}) y^2}{(\epsilon + \tau y)^2}\Big). \end{aligned}$$

This gives (3.18). On the other hand,

$$\begin{aligned} |\tan\theta - \frac{\pi}{N}(\hat{x}_2 - \hat{x}_1)| &= |\frac{x_2 - \frac{\pi}{N} x_1 (\hat{x}_2 - \hat{x}_1)}{x_1}| \\ &\lesssim \frac{(\epsilon + \tau y)(2 \sin \frac{\pi}{2N} - \frac{\pi}{N}) + O((\epsilon + \tau) N^{-3})}{(\epsilon + \tau y)(1 + O(N^{-2}))} y \\ &\lesssim N^{-3}, \end{aligned}$$

which gives (3.19). Next consider $\det \nabla \boldsymbol{x}$. It follows from (3.4)-(3.6), (3.8) and $z \le y^2/4 \le y/4$ that

$$\det \nabla \boldsymbol{x} = 2 t_2 \hat{\alpha}_2 + O((\epsilon + \tau)\tau N^{-3} + \epsilon^2 N^{-5}) y.$$

Note that $\hat{\alpha}_2 = \tau(1 + O(N^{-2} + \frac{\epsilon}{\tau} N^{-4}))$, $t_2 = 2(\epsilon + \tau y + 2\tau \sin^2 \frac{\pi}{4N}) \sin \frac{\pi}{2N}(1 + O(N^{-2}))$, thus (3.20) follows.

For the type B element, by (3.10)-(3.13),

$$\begin{aligned} x_1 &= \epsilon + (\tau - 4\tau \sin^2 \frac{\pi}{4N} y - 8\epsilon \sin^4 \frac{\pi}{4N} y)(1 - y) - 2\epsilon \sin^2 \frac{\pi}{2N}(y^2 - 4z), \\ x_2 &= \big(- 2 \sin \frac{\pi}{2N}(\epsilon + \tau(1 - y)) - 4\epsilon \sin \frac{\pi}{2N} \sin^2 \frac{\pi}{4N}(1 - 2y)\big)(\hat{x}_2 - \hat{x}_1), \end{aligned}$$

which gives (3.21), (3.22). While by (3.15),

$$\begin{aligned} &\det \nabla \boldsymbol{x} \\ &= 4\tau \sin \frac{\pi}{2N}\big((\epsilon + \tau(1 - y)) + (2y^2 - 3y + 1) O(\tau N^{-2}) + O(\epsilon N^{-2} + \frac{\epsilon^2}{\tau} N^{-4})\big) \\ &= 4\tau \sin \frac{\pi}{2N}(\epsilon + \tau(1 - y))\big(1 + O(N^{-2} + \frac{\epsilon}{\tau} N^{-4}) + \frac{2y^2 - 3y + 1}{\epsilon + \tau(1 - y)} O(\tau N^{-2})\big). \end{aligned}$$

Since $\sup\limits_{0\le y\le 1}|\frac{2y^2-3y+1}{\epsilon+\tau(1-y)}| = \sup\limits_{0\le y\le 1}|\frac{(2y-1)y}{\epsilon+\tau y}| \le \frac{1}{\epsilon+\tau}$, then we obtain (3.23).

For the type C element, by (3.16),

$$\begin{aligned} x_1 &= \epsilon + \tau\hat{x}_1 - 8\epsilon\sin^4\frac{\pi}{4N}\hat{x}_2 - 8\epsilon\cos\frac{\pi}{2N}\sin^2\frac{\pi}{4N}\hat{x}_2^2 - 4\tau\sin^2\frac{\pi}{4N}\hat{x}_1\hat{x}_2, \\ x_2 &= 2\sin\frac{\pi}{2N}\hat{x}_2(\epsilon+\tau\hat{x}_1) + 4\epsilon\sin\frac{\pi}{2N}\sin^2\frac{\pi}{4N}\hat{x}_2(1-2\hat{x}_2), \end{aligned}$$

which gives (3.24), (3.25). Meanwhile, one has

$$\det\nabla\boldsymbol{x} = 2\tau\sin\frac{\pi}{2N}\big(\epsilon+\tau\hat{x}_1+2\epsilon\sin^2\frac{\pi}{4N}(1-6\hat{x}_2+8\hat{x}_2^2)\big),$$

which leads to (3.26).

Similar arguments yield (3.27)-(3.29) for the type D element. □

Theorem 3.2 *The error between a cavity deformation* $\boldsymbol{u}(\boldsymbol{x}) = \frac{r(|\boldsymbol{x}|)}{|\boldsymbol{x}|}\boldsymbol{x} = (r(R),\theta)$ *and its interpolation function* $\Pi\boldsymbol{u}$ *satisfies*

$$\theta - \varphi = O(\tau^2N^{-1} + N^{-3}), \tag{3.34}$$

$$r(R) - \zeta = O(\tau^3 + \epsilon\tau N^{-2} + N^{-4}), \tag{3.35}$$

where the constants in $O(\cdot)$ *depend on* $\|r\|_\infty$, $\|r''\|_\infty$, $\|r^{(3)}\|_\infty$, $\inf r(R)$, $\sup\frac{r'(R)}{R}$.

Proof. For a typical type A element as used above, denote $\boldsymbol{X} = \Pi\boldsymbol{u}(\boldsymbol{x}) = (X_1, X_2)$, where $\boldsymbol{x} = F_T(\hat{\boldsymbol{x}})$. Some tedious manipulation yields that $X_1 = T_1 + T_2 z$, $X_2 = T_3(\hat{x}_2 - \hat{x}_1)$, where

$$\begin{aligned} &T_1 = r(\epsilon) + \alpha_2 y + \alpha_4 y^2, \quad T_2 = 2\gamma y - \beta, \quad T_3 = 8r(\epsilon+\tau)\sin^2\frac{\pi}{2N}, \\ &\alpha_4 = -4r(\epsilon+\frac{\tau}{2})\cos\frac{\pi}{2N} + 2r(\epsilon) + 2r(\epsilon+\tau)\cos\frac{\pi}{N}, \\ &\hat{\alpha}_4 = 2\epsilon + 2(\epsilon+\tau)\cos\frac{\pi}{N} - 4(\epsilon+\frac{\tau}{2})\cos\frac{\pi}{2N}, \end{aligned}$$

and where α_2, β, γ are given by (3.4)-(3.6). By the Taylor expansion,

$$\alpha_2 = r'(\epsilon)\tau + O(\tau^3 + \tau^2N^{-2} + \epsilon\tau N^{-2} + N^{-4}), \tag{3.36}$$

$$\alpha_4 = \frac{r''(\epsilon)}{2}\tau^2 - 2r(\epsilon)\sin^2\frac{\pi}{2N} + O(\tau^3 + \tau^2N^{-2} + \epsilon\tau N^{-2} + N^{-4}), \tag{3.37}$$

$$\beta = -2r(\epsilon)\sin\frac{\pi}{2N} + O(\tau^2N^{-1} + N^{-3}), \tag{3.38}$$

$$\gamma = r'(\epsilon)\tau\sin\frac{\pi}{2N} + O(\tau^2N^{-1} + N^{-3}). \tag{3.39}$$

Hence

$$\begin{aligned} T_1 &= r(\epsilon+\tau y) - 2r(\epsilon)y^2 \sin^2\frac{\pi}{2N} + O(\tau^3 + \tau^2 N^{-2} + \epsilon\tau N^{-2} + N^{-4}), \\ T_2 &= 2r(\epsilon+\tau y)\sin\frac{\pi}{2N} + O(\tau^2 N^{-1} + N^{-3}), \\ \tan\varphi &= \frac{\hat{x}_2 - \hat{x}_1}{T_1 + T_3 z} T_2 \\ &= \frac{r(\epsilon+\tau y)\frac{\pi}{N}(1+O(\tau^2+N^{-2}))}{r(\epsilon+\tau y)(1+O(\tau^3+N^{-2}))}(\hat{x}_2 - \hat{x}_1) \\ &= \frac{\pi}{N}(\hat{x}_2 - \hat{x}_1) + O(\tau^2 N^{-1} + N^{-3}). \end{aligned}$$

This together with (3.19) gives (3.34). Thus (3.34) is established on the type A element.

Next we estimate $r(R)-\zeta$. Expand $\zeta^2 = X_1^2 + X_2^2 = (T_1+T_3 z)^2 + T_2^2(\hat{x}_2-\hat{x}_1)^2$ as follows

$$\begin{aligned} \zeta^2 &= (r(\epsilon+\tau y) - 2r(\epsilon)(y^2-4z)\sin^2\frac{\pi}{2N} + O(\epsilon\tau N^{-2} + \tau^3 + \tau^2 N^{-2} + N^{-4}))^2 \\ &\quad + (2r(\epsilon+\tau y)\sin\frac{\pi}{2N} + O(\tau^2 N^{-1} + N^{-3}))^2 (y^2 - 4z) \\ &= r^2(\epsilon+\tau y) + 4r(\epsilon+\tau y)(r(\epsilon+\tau y) - r(\epsilon))(y^2-4z)\sin^2\frac{\pi}{2N} + \\ &\quad O(\epsilon\tau N^{-2} + \tau^3 + \tau^2 N^{-2} + N^{-4}) \\ &= r^2(\epsilon+\tau y) + O(\epsilon\tau N^{-2} + \tau^3 + \tau^2 N^{-2} + N^{-4}). \end{aligned}$$

Hence it follows from (3.18) and $r'(R) \le MR$ that (3.35) holds on the type A element.

Similarly, we can show that (3.34)-(3.35) hold on elements of types B, C and D. □

3.3 The error on the Jacobian determinant

Theorem 3.3 *The error between the Jacobian determinants of a cavity deformation* $\boldsymbol{u}(\boldsymbol{x}) = \frac{r(|\boldsymbol{x}|)}{|\boldsymbol{x}|}\boldsymbol{x} = (r(R),\theta)$ *and its interpolation function* $\Pi\boldsymbol{u}$ *satisfies*

$$\det\frac{\partial \Pi\boldsymbol{u}}{\partial \boldsymbol{x}}(\hat{\boldsymbol{x}}) - \det\frac{\partial \boldsymbol{u}}{\partial \boldsymbol{x}}(\hat{\boldsymbol{x}}) = \frac{O(\tau^3 N^{-1} + (\epsilon+\tau)\tau N^{-3} + N^{-5})}{\det\nabla\boldsymbol{x}} \quad (3.40)$$

$$= O\Big(N^{-2} + \frac{\tau^2}{\epsilon} + \frac{N^{-4}}{\epsilon\tau}\Big). \quad (3.41)$$

Proof. For the representative element of type A, it follows from (3.8), (3.36)-(3.39) and

$$\alpha_1 - r(\epsilon+\tau)\sin^2\frac{\pi}{2N} = r''(\epsilon+\frac{\tau}{2})\frac{\tau^2}{4} + O(\tau^4 + (\epsilon+\tau)\tau N^{-2} + N^{-4}),$$

that

$$\begin{aligned}\det\frac{\partial\Pi\boldsymbol{u}}{\partial\hat{\boldsymbol{x}}} &= -2\beta(\alpha_2 + 4(\alpha_1 - r(\epsilon+\tau)\sin^2\frac{\pi}{2N})y) + 4\gamma\alpha_2 y \\ &\quad + O(\tau^4N^{-1} + \epsilon\tau^3N^{-1} + \tau^2N^{-3} + \epsilon\tau N^{-3} + N^{-5}) \\ &= 4\tau\sin\frac{\pi}{2N}r(\epsilon+\tau y)r'(\epsilon+\tau y) + O(\tau^3N^{-1} + (\epsilon+\tau)\tau N^{-3} + N^{-5}),\end{aligned}$$

which gives (3.40). Hence by (3.20),

$$\begin{aligned}\det\frac{\partial\Pi\boldsymbol{u}}{\partial\boldsymbol{x}}(\hat{\boldsymbol{x}}) &= \frac{r(\epsilon+\tau y)r'(\epsilon+\tau y) + O(\tau^2 + (\epsilon+\tau)N^{-2} + \tau^{-1}N^{-4})}{(\epsilon+\tau y)\big(1 + O(\frac{\epsilon+\tau}{\epsilon}N^{-2} + \frac{\epsilon}{\tau}N^{-4})\big)} \\ &= \frac{r(\epsilon+\tau y)r'(\epsilon+\tau y)}{\epsilon+\tau y} + O\Big(\frac{\tau^2}{\epsilon} + \frac{\epsilon+\tau}{\epsilon}N^{-2} + \frac{N^{-4}}{\epsilon\tau}\Big).\end{aligned}$$

On the other hand , it follows from (3.18) that

$$\det\frac{\partial\boldsymbol{u}}{\partial\boldsymbol{x}}(\hat{\boldsymbol{x}}) = \frac{r(R)r'(R)}{R} = \frac{r(\epsilon+\tau y)r'(\epsilon+\tau y)}{\epsilon+\tau y} + O(N^{-2}).$$

Hence

$$\det\frac{\partial\Pi\boldsymbol{u}}{\partial\boldsymbol{x}}(\hat{\boldsymbol{x}}) - \det\frac{\partial\boldsymbol{u}}{\partial\boldsymbol{x}}(\hat{\boldsymbol{x}}) = O\Big(\frac{\tau^2}{\epsilon} + \frac{\epsilon+\tau}{\epsilon}N^{-2} + \frac{N^{-4}}{\epsilon\tau}\Big).$$

Since $\frac{\tau^2}{\epsilon} + \frac{N^{-4}}{\epsilon\tau} \geq 2\sqrt{\frac{\tau}{\epsilon^2}N^{-4}} = 2\frac{\sqrt{\tau}}{\epsilon}N^{-2} > \frac{\tau}{\epsilon}N^{-2}$, thus (3.41) holds on type A elements.

The proof for types B, C, D elements is similar. □

Remark 3.4 *The results above imply that, if there exits a constant $d > 0$ such that $\det\frac{\partial\boldsymbol{u}}{\partial\boldsymbol{x}} \geq d$ which is in fact the case for the radially symmetric cavity solution, then there exist $C_1 > 0$, $C_2 > 0$, $C_3 > 0$ such that $\det\frac{\partial\Pi\boldsymbol{u}}{\partial\boldsymbol{x}} > 0$ as long as $\tau \leq C_1\epsilon^{1/2}$ and $N^{-1} \leq \min\{C_2(\epsilon\tau)^{1/4}, C_3\}$, which is in a good agreement with the result obtained in [33] for the orientation-preservation condition.*

3.4 The error on the elastic energy

Let $\mathcal{J}(\Omega_{(\epsilon,\tau)})$ be a quadratic iso-parametric finite element triangulation of $\Omega_{(\epsilon,\tau)}$ consisting of either a layer of evenly distributed elements of types A and B as shown in Figure 5(a), or a layer of evenly distributed elements of types A, C and D as shown in Figure 5(b), and the corresponding elements are denoted by T_A, T_B, T_C and T_D accordingly. Let $\Omega^{\mathcal{J}}_{(\epsilon,\tau)} = \cup_{T\in\mathcal{J}(\Omega_{(\epsilon,\tau)})}T$. For the energy density function of the form (1.3), $S \subset \mathbb{R}^2$, denote

$$E_1(\boldsymbol{u}; S) = \omega \int_S |\nabla \boldsymbol{u}|^p \, d\boldsymbol{x}, \tag{3.42}$$

$$E_2(\boldsymbol{u}; S) = \int_S g\,(\det \nabla \boldsymbol{u})\, d\boldsymbol{x}, \tag{3.43}$$

$$A(\epsilon,\tau) = (2-p)\int_\epsilon^{\epsilon+\tau} t^{1-p}dt = (\epsilon+\tau)^{2-p} - \epsilon^{2-p}. \tag{3.44}$$

Let $E_i(\Pi\boldsymbol{u}; \Omega^{\mathcal{J}}_{(\epsilon,\tau)})$, $E(\Pi\boldsymbol{u}; \Omega^{\mathcal{J}}_{(\epsilon,\tau)})$ be the corresponding counterparts of the elastic energy of $\Pi\boldsymbol{u}$ on the elements in $\Omega_{(\epsilon,\tau)}$. Then, we have the following result.

Theorem 3.5 *The elastic energies of a cavity deformation* $\boldsymbol{u}(\boldsymbol{x}) = \frac{r(|\boldsymbol{x}|)}{|\boldsymbol{x}|}\boldsymbol{x}$ *and its interpolation function* $\Pi\boldsymbol{u}$ *satisfy*

$$E_1(\Pi\boldsymbol{u}; \Omega^{\mathcal{J}}_{(\epsilon,\tau)}) = E_1(\boldsymbol{u}; \Omega^{\mathcal{J}}_{(\epsilon,\tau)})(1 + O(\tau^2 + N^{-2} + \frac{\epsilon}{\tau}N^{-4})), \tag{3.45}$$

$$E_2(\Pi\boldsymbol{u}; \Omega^{\mathcal{J}}_{(\epsilon,\tau)}) = E_2(\boldsymbol{u}; \Omega^{\mathcal{J}}_{(\epsilon,\tau)}) + O(\tau^3 + (\epsilon+\tau)\tau N^{-2} + N^{-4}), \tag{3.46}$$

$$E(\Pi\boldsymbol{u}; \Omega^{\mathcal{J}}_{(\epsilon,\tau)}) = E(\boldsymbol{u}; \Omega^{\mathcal{J}}_{(\epsilon,\tau)})(1 + O(\tau^2 + N^{-2} + \frac{N^{-4}}{\tau})), \tag{3.47}$$

$$E(\boldsymbol{u}; \Omega^{\mathcal{J}}_{(\epsilon,\tau)}) = E(\boldsymbol{u}; \Omega_{(\epsilon,\tau)})(1 + O(\tau^2 + N^{-2} + \frac{\epsilon}{\tau}N^{-4})) \sim A(\epsilon,\tau). \tag{3.48}$$

Proof. On an element of type A, it follows from (3.7) that

$$\nabla\Pi\boldsymbol{u}(\boldsymbol{x}) = \frac{\partial\Pi\boldsymbol{u}}{\partial\hat{\boldsymbol{x}}}(\nabla\boldsymbol{x})^{-1} = \frac{1}{\det\nabla\boldsymbol{x}}\begin{pmatrix} A_{11} & A_{12} \\ A_{21} & A_{22}\end{pmatrix},$$

where by (3.36)-(3.39), one has

$$\begin{aligned}
A_{11} &= 4\tau \sin\frac{\pi}{2N}(r'(\epsilon)(\epsilon+\tau y)+r''(\epsilon+\tau/2)\epsilon\tau y)+O(\tau^3N^{-1}+\tau N^{-3}+\epsilon N^{-5}) \\
&= 4r'(\epsilon+\tau y)(\epsilon+\tau y)\tau\sin\frac{\pi}{2N}+O(\tau^3N^{-1}+\tau N^{-3}+\epsilon N^{-5}), \\
A_{12} &= O(\tau N^{-2}), \\
A_{21} &= O(\tau N^{-2}), \\
A_{22} &= 4r(\epsilon+\tau y)\tau\sin\frac{\pi}{2N}+O(\tau^3N^{-1}+\tau N^{-3}+\epsilon N^{-5}),
\end{aligned}$$

where $y=\hat{x}_1+\hat{x}_2$, $\hat{\boldsymbol{x}}=F_T^{-1}(\boldsymbol{x})$. Thus, denote $\xi_A(y)=\epsilon+\tau y$ and $\Upsilon(y)=r^2(\xi_A(y))+r'(\xi_A(y))^2\xi_A(y)^2$, one has

$$\Big|\frac{\partial\Pi\boldsymbol{u}}{\partial\boldsymbol{x}}\Big|^2=\frac{1}{(\det\nabla\boldsymbol{x})^2}\sum_{i,j}A_{ij}^2=\frac{(4\tau\sin\frac{\pi}{2N})^2}{(\det\nabla\boldsymbol{x})^2}\Upsilon(y)(1+\iota_1),$$

where $\iota_1=O(\tau^2+N^{-2}+\frac{\epsilon}{\tau}N^{-4})$. Hence

$$\Big|\frac{\partial\Pi\boldsymbol{u}}{\partial\boldsymbol{x}}\Big|^p=\frac{(4\tau\sin\frac{\pi}{2N})^p}{(\det\nabla\boldsymbol{x})^p}\Upsilon(y)^{p/2}(1+\iota_1).$$

It follows from Lemma 3.1 or more precisely (3.20) that

$$\begin{aligned}
&\int_{T_A}\Big|\frac{\partial\Pi\boldsymbol{u}}{\partial\boldsymbol{x}}\Big|^p d\boldsymbol{x}=\int_{\hat{T}}\Big|\frac{\partial\Pi\boldsymbol{u}}{\partial\boldsymbol{x}}\Big|^p\det\nabla\boldsymbol{x}d\hat{\boldsymbol{x}} \\
=\;& 4\tau\sin\frac{\pi}{2N}\int_{\hat{T}}\Upsilon(y)^{p/2}(\xi_A(y)+2\tau\sin^2\frac{\pi}{4N})^{1-p}d\hat{\boldsymbol{x}}(1+\iota_1) \\
=\;& 4\tau\sin\frac{\pi}{2N}\int_0^1 y\Upsilon(y)^{p/2}(\xi_A(y)+2\tau\sin^2\frac{\pi}{4N})^{1-p}dy(1+\iota_1),
\end{aligned}$$

where $\hat{T}$ is the reference element as Figure 1. Similarly, by Lemma 3.1 or more precisely (3.23), on the element of type B, one has

$$\begin{aligned}
\int_{T_B}\Big|\frac{\partial\Pi\boldsymbol{u}}{\partial\boldsymbol{x}}\Big|^p d\boldsymbol{x} &= 4\tau\sin\frac{\pi}{2N}\int_0^1 y\Upsilon(1-y)^{p/2}\xi_A(1-y)^{1-p}dy(1+\iota_1) \\
&= 4\tau\sin\frac{\pi}{2N}\int_0^1(1-y)\Upsilon(y)^{p/2}\xi_A(y)^{1-p}dy(1+\iota_1). \quad (3.49)
\end{aligned}$$

Thus

$$\int_{T_A\cup T_B}\Big|\frac{\partial\Pi\boldsymbol{u}}{\partial\boldsymbol{x}}\Big|^p d\boldsymbol{x}=4\tau\sin\frac{\pi}{2N}\int_0^1\Upsilon(y)^{p/2}\xi_A(y)^{1-p}dy(1+\iota_1)+\digamma,$$

where by the median formula,

$$\begin{aligned}
|F| &= 4\tau \sin\frac{\pi}{2N}\int_0^1 y\Upsilon(y)^{p/2}\Big(\xi_A(y)^{1-p} - (\xi_A(y) + 2\tau\sin^2\frac{\pi}{4N})^{1-p}\Big)dy \\
&\le 4(p-1)\tau\sin\frac{\pi}{2N}\int_0^1 y\Upsilon(y)^{p/2}\xi_A(y)^{-p}2\tau\sin^2\frac{\pi}{4N}dy \\
&< 4(p-1)\tau\sin\frac{\pi}{2N}\sin^2\frac{\pi}{4N}\int_0^1 \Upsilon(y)^{p/2}\xi_A(y)^{1-p}dy.
\end{aligned}$$

This yields that

$$\int_{T_A\cup T_B}\left|\frac{\partial\Pi\boldsymbol{u}}{\partial\boldsymbol{x}}\right|^p d\boldsymbol{x} = 4\tau\sin\frac{\pi}{2N}\int_0^1 \Upsilon(y)^{p/2}\xi_A(y)^{1-p}dy(1+\iota_1). \tag{3.50}$$

Similar calculations yield

$$\left|\frac{\partial\Pi\boldsymbol{u}}{\partial\boldsymbol{x}}\right|^p = \frac{(2\tau\sin\frac{\pi}{2N})^p}{(\det\nabla\boldsymbol{x})^p}\Upsilon(\hat{x}_1)^{p/2}(1+O(\tau^2+N^{-2})),$$

and

$$\left|\frac{\partial\Pi\boldsymbol{u}}{\partial\boldsymbol{x}}\right|^p = \frac{(2\tau\sin\frac{\pi}{2N})^p}{(\det\nabla\boldsymbol{x})^p}\Upsilon(\hat{x}_2)^{p/2}(1+O(\tau^2+N^{-2})),$$

on the elements of types C and D respectively. Thus it follows from Lemma 3.1 or more precisely (3.26) and (3.29) that

$$\begin{aligned}
&\int_{T_C\cup T_D}\left|\frac{\partial\Pi\boldsymbol{u}}{\partial\boldsymbol{x}}\right|^p d\boldsymbol{x} \\
&= 2\tau\sin\frac{\pi}{2N}\int_{\hat{T}}\big(\Upsilon(\hat{x}_1)^{p/2}\xi_A(\hat{x}_1)^{1-p} + \Upsilon(\hat{x}_2)^{p/2}\xi_A(\hat{x}_2)^{1-p}\big)d\hat{\boldsymbol{x}}(1+O(\tau^2+N^{-2})) \\
&= 4\tau\sin\frac{\pi}{2N}\int_0^1 (1-y)\Upsilon(y)^{p/2}\xi_A(y)^{1-p}dy(1+O(\tau^2+N^{-2})).
\end{aligned}$$

Comparing this with the corresponding estimate on element T_B (compare (3.49)), we are led to (compare (3.50))

$$\int_{T_A\cup T_C\cup T_D}\left|\frac{\partial\Pi\boldsymbol{u}}{\partial\boldsymbol{x}}\right|^p d\boldsymbol{x} = 4\tau\sin\frac{\pi}{2N}\int_0^1 \Upsilon(y)^{p/2}\xi_A(y)^{1-p}dy(1+\iota_1). \tag{3.51}$$

Similarly, by Lemma 3.1, one has

$$\begin{aligned}
\int_{T_A}\left|\frac{\partial \boldsymbol{u}}{\partial \boldsymbol{x}}\right|^p d\boldsymbol{x} &= \int_{T_A}\left(r^2(|\boldsymbol{x}|)+r'(|\boldsymbol{x}|)^2|\boldsymbol{x}|^2\right)^{p/2}|\boldsymbol{x}|^{-p}d\boldsymbol{x}\\
&= \int_T \Upsilon(\hat{x}_1+\hat{x}_2)^{p/2}\xi_A(\hat{x}_1+\hat{x}_2)^{-p}\det\nabla\boldsymbol{x}\,d\hat{\boldsymbol{x}}(1+O(N^{-2}))\\
&= 4\tau\sin\frac{\pi}{2N}\int_0^1 y\Upsilon(y)^{p/2}\xi_A(y)^{-p}(\xi_A(y)+2\tau\sin^2\frac{\pi}{4N})dy(1+\iota_1),\\
\int_{T_B}\left|\frac{\partial \boldsymbol{u}}{\partial \boldsymbol{x}}\right|^p d\boldsymbol{x} &= 4\tau\sin\frac{\pi}{2N}\int_0^1 y\Upsilon(1-y)^{p/2}\xi_A(1-y)^{1-p}dy(1+\iota_1)\\
&= 4\tau\sin\frac{\pi}{2N}\int_0^1 (1-y)\Upsilon(y)^{p/2}\xi_A(y)^{1-p}dy(1+\iota_1),
\end{aligned}$$

which yield

$$\begin{aligned}
\int_{T_A\cup T_B}\left|\frac{\partial \boldsymbol{u}}{\partial \boldsymbol{x}}\right|^p d\boldsymbol{x} &= 4\tau\sin\frac{\pi}{2N}\int_0^1 \Upsilon(y)^{p/2}\xi_A(y)^{1-p}dy(1+\iota_1)\\
&\quad +4\tau\sin\frac{\pi}{2N}\int_0^1 y\Upsilon(y)^{p/2}\xi_A(y)^{-p}2\tau\sin^2\frac{\pi}{4N}dy\\
&= 4\tau\sin\frac{\pi}{2N}\int_0^1 \Upsilon(y)^{p/2}\xi_A(y)^{1-p}dy(1+\iota_1), \qquad (3.52)
\end{aligned}$$

or, since $T_B = T_C \cup T_D$, equivalently

$$\int_{T_A\cup T_C\cup T_D}\left|\frac{\partial \boldsymbol{u}}{\partial \boldsymbol{x}}\right|^p d\boldsymbol{x} = 4\tau\sin\frac{\pi}{2N}\int_0^1 \Upsilon(y)^{p/2}\xi_A(y)^{1-p}dy(1+\iota_1). \qquad (3.53)$$

Thus (3.45) follows as a direct consequence of (3.50)-(3.53). Moreover,

$$\begin{aligned}
E_1(\boldsymbol{u};\Omega^{\mathcal{J}}_{(\epsilon,\tau)}) &= 4\omega\tau N\sin\frac{\pi}{2N}\int_0^1 \Upsilon(y)^{p/2}\xi_A(y)^{1-p}dy(1+\iota_1)\\
&= 2\pi\omega\tau\int_0^1 \Upsilon(y)^{p/2}\xi_A(y)^{1-p}dy(1+\iota_1)\\
&= 2\pi\omega\int_\epsilon^{\epsilon+\tau}(r^2(t)+r'(t)^2t^2)^{p/2}t^{1-p}dt(1+\iota_1)\\
&= E_1(\boldsymbol{u};\Omega_{(\epsilon,\tau)})(1+\iota_1)\\
&\sim A(\epsilon,\tau).
\end{aligned}$$

Thus we get

$$E_1(\boldsymbol{u};\Omega^{\mathcal{J}}_{(\epsilon,\tau)}) = E_1(\boldsymbol{u};\Omega_{(\epsilon,\tau)})(1+O(\tau^2+N^{-2}+\frac{\epsilon}{\tau}N^{-4}))\sim A(\epsilon,\tau).$$

On the other hand, by (3.40) and $g(\cdot) \in C^2(0,+\infty)$, on the elements of types A, B, C and D, we have

$$g\Big(\det \frac{\partial \Pi \boldsymbol{u}}{\partial \boldsymbol{x}}\Big) = g(\det \frac{\partial \boldsymbol{u}}{\partial \boldsymbol{x}}) + \frac{N^{-1}\iota_2}{\det \nabla \boldsymbol{x}},$$

where $\iota_2 = O(\tau^3 + (\epsilon+\tau)\tau N^{-2} + N^{-4})$. Hence

$$|E_2(\Pi \boldsymbol{u}; \Omega^{\mathcal{J}}_{(\epsilon,\tau)}) - E_2(\boldsymbol{u}; \Omega^{\mathcal{J}}_{(\epsilon,\tau)})| = N \int_{T_A \cup T_B} \frac{1}{\det \nabla \boldsymbol{x}} d\boldsymbol{x} N^{-1}\iota_2 = \iota_2,$$

which is (3.46). Similar arguments and the fact that $g(\det \nabla \boldsymbol{u}) \geq g_0 > 0$ lead to

$$E_2(\boldsymbol{u}; \Omega^{\mathcal{J}}_{(\epsilon,\tau)}) = E_2(\boldsymbol{u}; \Omega_{(\epsilon,\tau)})(1+\iota_1) \sim \epsilon\tau + \tau^2,$$

hence (3.48) holds, i.e., $E(\boldsymbol{u}; \Omega^{\mathcal{J}}_{(\epsilon,\tau)}) \sim E(\boldsymbol{u}; \Omega_{(\epsilon,\tau)}) \sim A(\epsilon,\tau) \sim \max\{\epsilon,\tau\}^{1-p}\tau$. Thus, one has

$$\frac{|E_2(\Pi \boldsymbol{u}; \Omega^{\mathcal{J}}_{(\epsilon,\tau)}) - E_2(\boldsymbol{u}; \Omega^{\mathcal{J}}_{(\epsilon,\tau)})|}{E(\boldsymbol{u}; \Omega^{\mathcal{J}}_{(\epsilon,\tau)})} = \frac{\iota_2}{A(\epsilon,\tau)} \sim \max\{\epsilon,\tau\}^{p-1}\iota_2/\tau,$$

which together with (3.45) gives (3.47). □

4 Meshing strategy and convergence theorem

In this section, by applying the error estimates given in § 3 and the orientation-preservation condition given in [33] (see also Remark 3.4), we first establish a meshing strategy on the domain $\Omega_{\epsilon_0} = B_1(\mathbf{0}) \setminus B_{\epsilon_0}(\mathbf{0})$. The mesh is assumed to be introduced by $\mathcal{J} = \bigcup_{i=0}^{m} \Omega^{\mathcal{J}}_{(\epsilon_i,\tau_i)}$ with each $\Omega^{\mathcal{J}}_{(\epsilon_i,\tau_i)}$ being either a radially symmetric mesh on a circular ring domain $\{x : \epsilon_i \leq |x| \leq \epsilon_{i+1}\}$ consisting of $2N_i$ iso-parametric quadratic finite elements of types A and B as shown in Figure 5(a), or a slightly modified mesh consisting of $3N_i$ iso-parametric quadratic finite elements of types A, C and D as shown in Figure 5(b). Our purpose is, given a far field reference mesh size $h > 0$, to find m, and ϵ_i, N_i, $i = 0, 1, \cdots, m$, so that (1): the finite element interpolation function of the cavity deformation is orientation preserving; (2): the relative errors of the elastic energy E on the

circular ring domains $\{x : \epsilon_i \le |x| \le \epsilon_{i+1}\}$ are all of the order $O(h^2)$; and (3): at the same time, the absolute errors of the elastic energy on each of the circular domains are of the same order. The last requirement, which can be realized by making $(\epsilon_i + \tau_i)^{2-p} - \epsilon_i^{2-p} \sim E_1(\boldsymbol{u}; \Omega_{(\epsilon_i,\tau_i)}) \sim E(\boldsymbol{u}; \Omega_{(\epsilon_i,\tau_i)})$ (see (3.48)) to be the same order, implies that the absolute error of the elastic energy is in some sense equi-distributed in the radial direction.

Let $\epsilon_0 < \epsilon_1 \cdots < \epsilon_i < \cdots < \epsilon_m < \epsilon_{m+1} = 1.0$, let $\tau_i = \epsilon_{i+1} - \epsilon_i$, and let N_i be the number of the nodes on both the inner and outer boundaries of the circular ring domain $\Omega_{(\epsilon_i,\tau_i)}$ introduced by $\Omega^{\mathcal{J}}_{(\epsilon_i,\tau_i)}$ (see Figure 5(a)). For the simplicity of the finite element coding, we require that either $N_i = 2N_{i+1}$ or $N_i = N_{i+1}$. By Theorem 3.7 of [33] (see also Remark 3.4), to preserve the orientation of the finite element interpolation functions, ϵ_i, τ_i, N_i must satisfy the conditions $\tau_i \le C_1\epsilon_i^{1/2}$, and $N_i^{-1} \le C_2(\epsilon_i\tau_i)^{1/4}$, where C_1, C_2 are constants depending on the solution $r(R)$. On the other hand, by (3.47), to ensure the relative error of $E(\Pi\boldsymbol{u}; \Omega^{\mathcal{J}}_{(\epsilon_i,\tau_i)})$ to be the order of $O(h^2)$, a necessary condition is that $\tau_i = O(h)$, $\forall i$. Moreover, since $A(\epsilon_m, \tau_m) = 1 - (1-\tau_m)^{2-p} \le (2-p)2^{p-1}\tau_m = O(h)$ if $\epsilon_m > \frac{1}{2}$, it is natural to require $A(\epsilon_i, \tau_i) \le Ch$, for all $0 \le i \le m$, which imposes a condition on the layer's thickness: $\tau_i \le d(\epsilon_i, h)$, where $d(x,h) := (x^{2-p} + Ch)^{\frac{1}{2-p}} - x$ is defined by $A(x, d(x,h)) = Ch$. As is shown in [34], $\tau_i \le d(\epsilon_i, h)$ leads to $\tau_i = O(h)$ as $h \to 0$.

For given positive constants C_1, C_2, $C \ge (2-p)2^{p-1}$, $h \le \min\{\frac{2-p}{2^{2-p}C}, \frac{2-p}{2^{p-1}C}\}$ (see [34]), $A_1 < A_2$ satisfying $[(A_2h)^{-1}, (A_1h)^{-1}] \cap \mathbb{Z}_+ \ne \emptyset$, the analysis above leads to the following meshing strategy.

A meshing strategy of $\{\Omega^{\mathcal{J}_h}_{(\epsilon_i,\tau_i)}\}_{i=0}^m$:

(1) Set $\tau_0 = \min\{C_1\epsilon_0^{1/2}, d(\epsilon_0, h)\}$. Take $\tilde{N}_m \in [(A_2h)^{-1}, (A_1h)^{-1}] \cap \mathbb{Z}_+$. Let $\bar{N}_0 = \min\{N \in \mathbb{Z}_+ : N^{-1} \le \min\{C_2(\epsilon_0\tau_0)^{1/4}, (C^2\tau_0h^2)^{1/4}\}\}$. Set $k = \min\{j : 2^j\tilde{N}_m \ge \bar{N}_0\}$, and $N_0 = 2^k\tilde{N}_m$.

(2) Set $k_0 = 0$. For $i \ge 1$, set $\epsilon_i = \epsilon_{i-1} + \tau_{i-1}$, and

$$\tau_i = \min\{1 - \epsilon_i, C_1\epsilon_i^{1/2}, d(\epsilon_i, h)\}. \tag{4.1}$$

If $\tau_i = 1 - \epsilon_i$, set $m = i$. The least admissible N_i such that $N_i^{-1} \leq \min\{C_2(\epsilon_i\tau_i)^{1/4}, (C^2\tau_i h^2)^{1/4}\}$ is determined as follows:

(i) If $k_{i-1} < k$, set $\bar{N}_i = \frac{N_{i-1}}{2}$. If $\bar{N}_i^{-1} \leq \min\{C_2(\epsilon_i\tau_i)^{1/4}, (C^2\tau_i h^2)^{1/4}\}$, then set $k_i = k_{i-1} + 1$, $N_i = \bar{N}_i$; otherwise, set $k_i = k_{i-1}$, $N_i = N_{i-1}$.

(ii) If $k_{i-1} = k$, set $k_i = k_{i-1}$, $N_i = N_{i-1}$.

(3) Whenever $N_i = 2N_{i+1}$ occurs, each type B element in the circular ring $\Omega^{\mathcal{J}}_{(\epsilon_i,\tau_i)}$ is divided into a pair of elements of types C and D by introducing a straight line right in the middle along the radial direction (see Figure 5(b)).

Remark 4.1 *The step (3) above can be viewed as a conforming process. The quadratic iso-parametric finite element function space established on a mesh produced according to the above meshing strategy is a conforming finite element function space. The analysis in § 3 shows that the orientation-preservation conditions as well as the error bounds of the interpolation function of the cavity deformation are not jeopardised by the conforming process.*

On a mesh $\{\Omega^{\mathcal{J}_h}_{(\epsilon_i,\tau_i)}\}_{i=0}^m$ produced according to the above meshing strategy, we have the following results.

Theorem 4.2 *Let $\Omega_h = \cup_{i=0}^m \Omega^{\mathcal{J}_h}_{(\epsilon_i,\tau_i)}$, let $\boldsymbol{u}(\boldsymbol{x})$ be the radially symmetric cavity deformation on Ω_{ϵ_0}, then $\det \nabla \Pi\boldsymbol{u}(\boldsymbol{x}) > 0$ a.e. on Ω_h. Moreover, the error of the elastic energy satisfies*

$$E(\Pi\boldsymbol{u}; \Omega_h) = \sum_{i=0}^{m} E(\Pi\boldsymbol{u}; \Omega^{\mathcal{J}_h}_{(\epsilon_i,\tau_i)}) = E(\boldsymbol{u}; \Omega_{\epsilon_0})(1 + O(h^2)). \tag{4.2}$$

Proof. Since $\tilde{N}_m \sim 1/h$, $N_i \geq \tilde{N}_m$, it follows that $N_i^{-1} = O(h)$. It is easily verified that the orientation-preservation conditions $\tau_i \leq C_1\epsilon_i^{1/2}$ and $N_i^{-1} \leq C_2(\epsilon_i\tau_i)^{1/4}$ are satisfied and $\tau_i = O(h), \frac{1}{\tau_i}N_i^{-4} = O(h^2)$. Thus, $\det \nabla \Pi\boldsymbol{u}(\boldsymbol{x}) > 0$ a.e. on Ω_h by Theorem 3.7 of [33] (see also Remark 3.4). On the other hand, it follows from (3.48) and (3.47) that, for all i, $E(\Pi\boldsymbol{u}; \Omega^{\mathcal{J}_h}_{(\epsilon_i,\tau_i)}) = E(\boldsymbol{u}; \Omega_{(\epsilon_i,\tau_i)})(1 + O(h^2))$, which yield (4.2). □

Theorem 4.3 *Let* $\Omega_{h_k} = \cup_{i=0}^{m}\Omega_{(\epsilon_i,\tau_i)}^{\mathcal{J}_{h_k}}$ *with* $\lim_{k\to\infty} h_k = 0$, *let* $\mathcal{A}_{h_k}$ *be the corresponding conforming finite element function spaces consist of piecewise quadratic iso-parametric functions satisfying the boundary condition* $\boldsymbol{v}_{h_k}(\boldsymbol{x}) = \lambda\boldsymbol{x}$ *for all the mesh nodes on the boundary* Γ_0, *and let* $\boldsymbol{u}_{h_k}$ *be a minimizer of* $E(\cdot)$ *in* $\mathcal{A}_{h_k}$. *Suppose that the radially symmetric cavity deformation* $\boldsymbol{u}$ *is the unique minimizer of* $E(\cdot)$ *in* $\mathcal{A}$, *then* $\boldsymbol{u}_{h_k}\chi_{\Omega_{\epsilon_0}} \to \boldsymbol{u}$ *in* $W^{1,p}(\Omega_{\epsilon_0},\mathbb{R}^2)$.

Proof. By Theorem 4.2 and the assumption that $\boldsymbol{u}$ is the energy minimizer, we conclude that

$$\lim_{k\to\infty} E(\boldsymbol{u}_{h_k}) = E(\boldsymbol{u}) = \inf_{\boldsymbol{v}\in\mathcal{A}} E(\boldsymbol{v}), \tag{4.3}$$

and in particular $\{\|\nabla\boldsymbol{u}_{h_k}\|_p\}$ is bounded, since $g > 0$. This, by the boundary condition and the Poincaré inequality [26], implies that $\{\boldsymbol{u}_{h_k}\chi_{\Omega_{\epsilon_0}}\}$ is bounded in $W^{1,p}(\Omega_{\epsilon_0},\mathbb{R}^2)$. Consequently, by the De La Vallée Poussin criterion ([24]), both $\{\nabla(\boldsymbol{u}_{h_k}\chi_{\Omega_{\epsilon_0}})\}$ and $\{\det\nabla(\boldsymbol{u}_{h_k}\chi_{\Omega_{\epsilon_0}})\}$ are equi-integrable, since $p > 1$ and g is a convex function satisfying (1.4). Thus, there exist a subsequence $\boldsymbol{u}_{h_k}\chi_{\Omega_{\epsilon_0}}$ (not relabelled), $\tilde{\boldsymbol{u}} \in W^{1,p}(\Omega_{\epsilon_0},\mathbb{R}^2)$ and $\vartheta \in L^1(\Omega_{\epsilon_0})$ such that

$$\boldsymbol{u}_{h_k}\chi_{\Omega_{\epsilon_0}} \rightharpoonup \tilde{\boldsymbol{u}} \in W^{1,p}(\Omega_{\epsilon_0},\mathbb{R}^2),\ \boldsymbol{u}_{h_k}\chi_{\Omega_{\epsilon_0}} \to \tilde{\boldsymbol{u}}\ a.e.,\ \det\nabla(\boldsymbol{u}_{h_k}\chi_{\Omega_{\epsilon_0}}) \rightharpoonup \vartheta \in L^1(\Omega_{\epsilon_0}).$$

Clearly $\vartheta \geq 0$ a.e., we claim that $\vartheta > 0$ a.e.. Suppose otherwise, i.e. if ϑ were zero in a set A of positive measure, then one would have $\int_A |\det\nabla\boldsymbol{u}_{h_k}| \to 0$ and $\det\nabla\boldsymbol{u}_{h_k} \to 0$ a.e. in A. Hence, by the assumption of g, one would have $g(\det\nabla\boldsymbol{u}_{h_k}) \to \infty$ a.e. in A, and as a consequence $E(\boldsymbol{u}_{h_k}) \to \infty$, which is a contradiction.

The fact that $\boldsymbol{u}_{h_k}\chi_{\Omega_{\epsilon_0}} \rightharpoonup \tilde{\boldsymbol{u}}$ in $W^{1,p}(\Omega_{\epsilon_0},\mathbb{R}^2)$ implies that $\nabla\boldsymbol{u}_{h_k}\chi_{\Omega_{\epsilon_0}} \rightharpoonup \nabla\tilde{\boldsymbol{u}}$ in $L^p(\Omega_{\epsilon_0},\mathbb{R}^{2\times2})$, $\operatorname{cof}\nabla\boldsymbol{u}_{h_k}\chi_{\Omega_{\epsilon_0}} \rightharpoonup \operatorname{cof}\nabla\tilde{\boldsymbol{u}}$ in $L^1(\Omega_{\epsilon_0},\mathbb{R}^{2\times2})$. In addition, since $\boldsymbol{u}_{h_k}$ is continuous, by Theorem 3 of [13], $\mathcal{E}(\boldsymbol{u}_{h_k}) = 0$, where

$$\mathcal{E}(\boldsymbol{v}) := \sup\{\mathcal{E}(\boldsymbol{v},\boldsymbol{f}) : \boldsymbol{f} \in C_c^\infty(\Omega\times\mathbb{R}^n,\mathbb{R}^n),\ ||\boldsymbol{f}||_\infty \leq 1\},$$

$$\mathcal{E}(\boldsymbol{v},\boldsymbol{f}) := \int_\Omega [\operatorname{cof}\nabla\boldsymbol{v}(\boldsymbol{x})\cdot\nabla_{\boldsymbol{x}}\boldsymbol{f}(\boldsymbol{x},\boldsymbol{v}(\boldsymbol{x})) + \det\nabla\boldsymbol{v}(\boldsymbol{x})\operatorname{div}_{\boldsymbol{v}}\boldsymbol{f}(\boldsymbol{x},\boldsymbol{v}(\boldsymbol{x}))]d\boldsymbol{x},$$

and where $\nabla_{\boldsymbol{x}}$ and $\operatorname{div}_{\boldsymbol{v}}$ denote the gradient and divergence of $f(\boldsymbol{x},\boldsymbol{v})$ with respect to $\boldsymbol{x}$ and $\boldsymbol{v}$ respectively. Thus, by Theorem 2 of [12] $\tilde{\boldsymbol{u}}$ is one-to-one

almost everywhere, and by Theorem 3 of [12] $\vartheta = \det \nabla \tilde{\boldsymbol{u}}$, a.e. and $\mathcal{E}(\tilde{\boldsymbol{u}}) = 0$. Moreover, by the boundary condition of $\boldsymbol{u}_{h_k}$ on Γ_0 and the relationship between Ω_{h_k} and Ω_{ϵ_0} we conclude that $\tilde{\boldsymbol{u}}|_{\Gamma_0} = \lim_{k\to\infty} \boldsymbol{u}_{h_k}|_{\Gamma_0} = \lambda \boldsymbol{x}$, hence $\tilde{\boldsymbol{u}} \in \mathcal{A}$. Thus, by the lower semi-continuity theorem ([2], Theorem 5.4) and (4.3), we obtain that $\inf\limits_{\boldsymbol{v}\in\mathcal{A}} E(\boldsymbol{v}) \le E(\tilde{\boldsymbol{u}}) \le \liminf\limits_{k\to\infty} E(\boldsymbol{u}_{h_k}) = \inf\limits_{\boldsymbol{v}\in\mathcal{A}} E(\boldsymbol{v})$, which implies that $\tilde{\boldsymbol{u}} = \boldsymbol{u}$ is the unique minimizer of $E(\cdot)$ in $\mathcal{A}$.

On the other hand, it follows from the convexity of g that

$$\begin{aligned} E(\boldsymbol{u}) - \omega \int_{\Omega_{\epsilon_0}} |\nabla \boldsymbol{u}|^p dxdx &= \int_{\Omega_{\epsilon_0}} g(\det \nabla \boldsymbol{u}) dx \\ &\le \liminf_{k\to\infty} \int_{\Omega_{\epsilon_0}} g(\det \nabla \boldsymbol{u}_{h_k}) dx \\ &= \liminf_{k\to\infty} (E(\boldsymbol{u}_{h_k}) - \omega \int_{\Omega_{\epsilon_0}} |\nabla \boldsymbol{u}_{h_k}|^p dx) \\ &= E(\boldsymbol{u}) - \omega \limsup_{k\to\infty} \int_{\Omega_{\epsilon_0}} |\nabla \boldsymbol{u}_{h_k}|^p dx. \end{aligned}$$

This implies that $\|\nabla \boldsymbol{u}\|_p = \lim\limits_{k\to\infty} \|\nabla \boldsymbol{u}_{h_k}\|_p$, which together with $\boldsymbol{u}_{h_k}\chi_{\Omega_{\epsilon_0}} \rightharpoonup \boldsymbol{u} \in W^{1,p}(\Omega_{\epsilon_0}, \mathbb{R}^2)$ yields $\boldsymbol{u}_{h_k}\chi_{\Omega_{\epsilon_0}} \to \boldsymbol{u} \in W^{1,p}(\Omega_{\epsilon_0}, \mathbb{R}^2)$ (see [8]). □

5 Numerical experiments and results

In this section, the numerical results are presented to illustrate the efficiency of our meshing strategy. Before proceeding, we notice that, in the meshing strategy, there are two solution-dependent constants C_1 and C_2, which are not known a priori. However, in applications, we can always start with $C_1 := d(\epsilon_0, h)\epsilon_0^{-1/2}$ and $C_2 := \tilde{N}_m^{-1}(\epsilon_0 d(\epsilon_0, h))^{-1/4}$, which are the least C_1 and C_2 such that the orientation-preservation conditions will practically not affect the mesh produced. The numerical solutions on an improper mesh with the constants C_1 or C_2 too large might still capture the cavitation phenomenon, but would typically fail to be orientation preserving, which can be most easily detected on the corners of the elements on the inner boundary of Ω_{ϵ_0}. Similar as in [34], whenever the failure of orientation preservation is detected, the constant C_1 or C_2 or both should be

reduced, say by half, or simply increase N_0 instead, say by doubling, and the process, repeat if necessary, will efficiently produce a proper mesh in the end.

The energy density in our numerical experiments is given by (1.3) with $p = 3/2$, $\omega = 2/3$, and $g(x) = 2^{-1/4}(\frac{1}{2}(x-1)^2 + \frac{1}{x})$, the domain is $\Omega_{\epsilon_0} = B_1(\mathbf{0}) \setminus B_{\epsilon_0}(\mathbf{0}) \subseteq \mathbb{R}^2$ with a displacement boundary condition $\boldsymbol{u}_0(\boldsymbol{x}) = 2\boldsymbol{x}$ given on $\Gamma_0 = \partial B_1(\mathbf{0})$ and a traction free boundary condition given on $\Gamma_1 = \{\boldsymbol{x} : |\boldsymbol{x}| = \epsilon_0\}$, and the meshes used are shown in Table 1 and Table 2, which are produced by the meshing strategy with $C = 2$, $C_1 = 0.9$, $C_2 = 0.5$, $A_1 = 0.8$, $A_2 = 1$ for $\epsilon_0 = 0.01$, $\epsilon_0 = 0.0001$ and various h.

Table 1: $\epsilon_0 = 0.01$.

h	$\min \tau_i$	$\max \tau_i$	m	N_h
0.06	0.0384	0.2112	7	15
0.04	0.0224	0.1504	11	20
0.03	0.0156	0.1164	14	27
0.02	0.0096	0.0768	22	40
0.01	0.0044	0.0396	44	80

Table 2: $\epsilon_0 = 0.0001$.

h	$\min \tau_i$	$\max \tau_i$	m	N_0	N_m
0.06	0.009	0.21	8	16	64
0.04	0.008	0.1488	12	20	80
0.03	0.0048	0.1128	16	27	108
0.02	0.0024	0.076	24	46	92
0.01	0.0008	0.0392	49	80	160

It happens that, for $\epsilon_0 = 0.01$, $N_i = N_h$ on each of the $m+1$ mesh layers, while for $\epsilon_0 = 0.0001$, the $N_i = 2N_{i+1}$ do occur in several of the innermost layers, however in both cases the total degrees of freedom N_d is asymptotically a quadratic function of h^{-1} as shown in Figure 6.

The convergence behavior of the elastic energy is shown in Figure 7, where it is clearly seen that the convergence rate of the elastic energy of the finite element solutions $\boldsymbol{u}_h$ is more than one order higher than that of one could standardly expect from a quadratic approximation (see also (3.47)) showing that the method probably has some kind of super-convergence potential. In Figure 8 and Figure 9, we see that $\|\boldsymbol{u} - \boldsymbol{u}_h\|_{0,2} = O(h^3)$ and $\|\boldsymbol{u} - \boldsymbol{u}_h\|_{1,p} = O(h^2)$ respectively, which show that our meshing strategy is optimal in the sense that the optimal order of

convergence rates in $\|\cdot\|_{0,2}$ and $\|\cdot\|_{1,p}$ norms can be achieved with the quadratic iso-parametric FEM, recalling that $N_d \sim h^{-2}$.

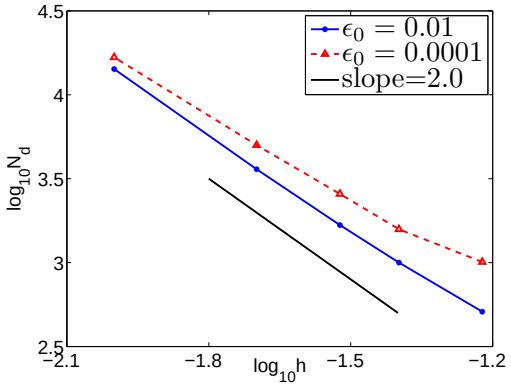

Figure 6: $N_d \sim h^{-2}$.

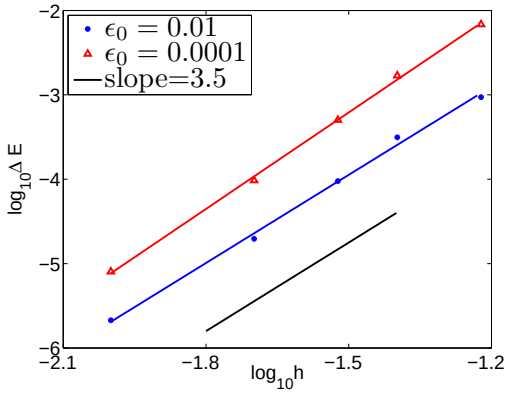

Figure 7: The energy error.

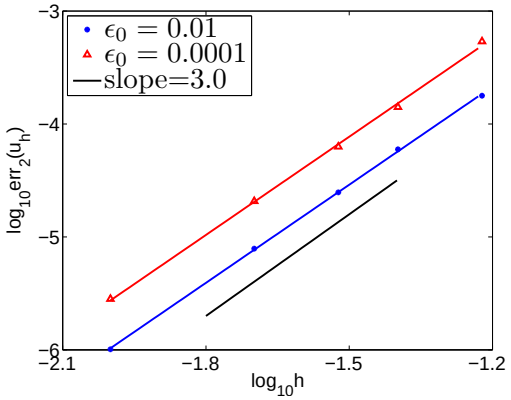

Figure 8: The L^2 error of $\boldsymbol{u}_h$.

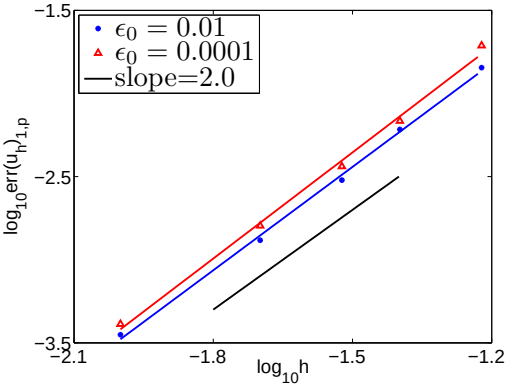

Figure 9: The $W^{1,p}$ error of $\boldsymbol{u}_h$.

Figure 10(a) compares the L^2 error of the numerical cavity solutions obtained on the meshes produced by our meshing strategy and on the meshes provided according to the limited numerical experiences given in [22]. Figure 10(b) displays the L^2 error of the numerical cavity solutions obtained by the quadratic iso-parametric FEM on the globally optimized meshes and locally optimized ones, where the mesh is optimized by using our meshing strategy only on $\{\boldsymbol{x} : \epsilon_0 \leq |\boldsymbol{x}| \leq 0.1\}$, and by the bi-quadratic dual-parametric FEM on the globally optimized meshes (see [34]), denoted in the legend as Iso-para-global, Iso-para-local and

Dual-para respectively. It is clearly seen that our meshing strategy efficiently works.

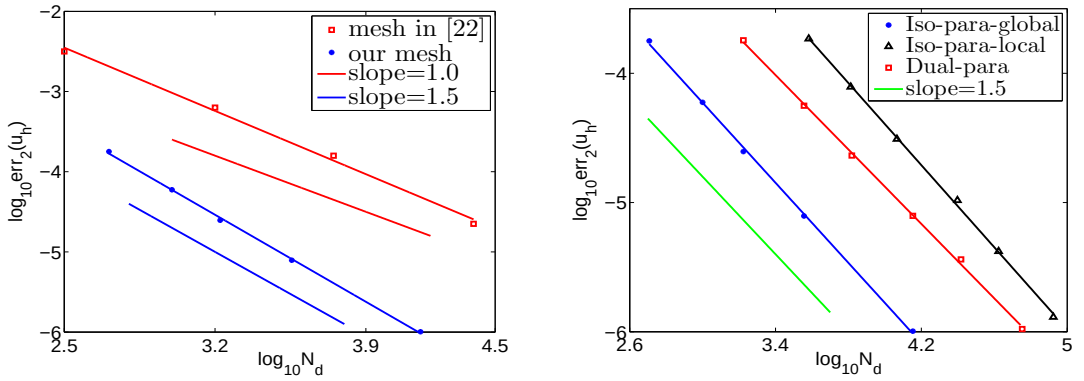

(a) Experience based vs. optimized meshes.

(b) Iso- and dual-parametric FEM.

Figure 10: The comparison of the L^2 errors of numerical solutions ($\epsilon_0 = 0.01$).

6 Concluding remarks

The error estimates obtained in this paper on the quadratic iso-parametric finite element interpolation functions of the cavity deformations enable us to establish the meshing strategy in a neighborhood of a pre-existing defect, and consequently to bound the error of the elastic energy of the conforming finite element cavity solutions in the order of $O(h^2)$, where h is the far field mesh size, and further to prove the convergence of the finite element solutions.

Our numerical experiments show that the convergence behavior of the finite element solutions in $W^{1,p}$ and L^2 norms with respect to h and N_d is essentially asymptotically independent of ϵ_0. In fact, for $\epsilon_0 = 10^{-2}$ and 10^{-4}, the errors in $W^{1,p}$ and L^2 norms drop to the levels below 10^{-3} and 10^{-5} respectively when $h = 0.01$ and N_d reaches about 1.6×10^4. Furthermore, the numerical experiments show that the rate of the elastic energy error of the numerical cavity solutions reaches the level of $O(h^{3.5})$, indicating that the numerical solutions obtained by the quadratic iso-parametric FEM on the meshes produced according to our meshing strategy might have certain super-convergence character, which yet

remains to be explored. The results suggest that the quadratic iso-parametric finite element method coupled with our meshing strategy could be considered as a reliable and efficient tool to compute the cavitation problems in nonlinear elasticity.

References

[1] Bai, Y., Li, Z., Numerical solution of nonlinear elasticity problems with laurentiev phenomenon. **Math. Models Methods Appl. Sci., 17** (2007), 1619-1640.

[2] Ball, J. M., Currie, J. C., Olver, P. J., Null Lagrangians, weak continuity, and variational problems of arbitary order. **J. Func. Anal., 41** (1981), 135-174.

[3] Ball, J. M., Discontinuous equilibrium solutions and cavitation in nonlinear elasticity. **Philos. Trans. R. Soc. London, A 306** (1982), 557-611.

[4] Ball, J. M., Knowles, G., A numerical method for detecting singular minimizers. **Numer. Math., 51** (1987), 181-197.

[5] Ciarlet, P. G., The finite element method for elliptic problems. Amsterdam: North-Holland (1978).

[6] Cristiano, A., Marcellan, A., Long, R., Hui, C.-Y., Stolk, J., Creton, C., An experimental investigation of fracture by cavitation of model elastomeric networks. **J. Polym. Sci. B Polym. Phys., 48(13)** (2010), 1409-1422.

[7] Dorfmann, A., Stress-softening of elastomers in hydrostatic tension. **Acta Mech., 165** (2003), 117-137.

[8] Evans, L. C., Gariepy, R. F., Some remarks concerning quasiconvexity and strong convergence. **Proc. Roy. Soc. Edin., 106A** (1987), 53-61.

[9] Gent, A. N., Lindley, P. B., International rupture of bounded rubber cylinders in tension. **Proc. Roy. Soc. London., A 249** (1958), 195-205.

[10] Hamdi, A., Guessasma, S., Abdelaziz, M. N., Fracture of elastomers by cavitation. **Mater. Des., 53** (2014), 497-503.

[11] Henao, D., Cavitation, invertibility, and convergence of regularized minimizers in nonlinear elasticity. **J. Elast., 94** (2009), 55-68.

[12] Henao, D., Mora-Corral, C., Invertibility and weak continuity of the determinant for the modelling of cavitation and fracture in nonlinear elasticity. **Arch. Rat. Mech. Anal., 197** (2010), 619-655.

[13] Henao, D., Mora-Corral, C., Fractute surfaces and the regularity of inverses for BV deformations. **Arch. Rat. Mech. Anal., 201** (2011), 575-629.

[14] Henao, D., Mora-Corral, C., Xu, X., Γ-convergence approximation of fracture and cavitation in nonlinear elasticity. **Arch. Rat. Mech. Anal., 216** (2015), 813-879.

[15] Henao, D., Mora-Corral, C., Xu, X., A numerical study of void coalescence and fracture in nonlinear elasticity. Preprint.

[16] Jaravel, J., Castagnet, S., Grandidier, J-C., Benoit, G., On key parameters influencing cavitation damage upon fast decompression in a hydrogen saturated elastomer. **Polym. Test, 30** (2013), 811-818.

[17] Kundu, S., Crosby, A. J., Cavitation and fracture behavior of polyacrylamide hydrogels. **Soft Matter, 5** (2009), 3963-3968.

[18] Lavrentiev, M., Sur quelques problems du calcul des variations. **Ann. Math. Pure Appl., 4** (1926), 7-28.

[19] Lefèvre, V., Ravi-Chandar, K., Lopez-Pamies, O., Cavitation inrubber: an elastic instability or a fracture phenomenon? **Int. J. Fract., 192** (2015), 1-23.

[20] Li, Z., A numerical method for computing singular minimizers. **Numer. Math., 71** (1995), 317-330.

[21] Lian, Y., Li, Z., A dual-parametric finite element method for cavitation in nonlinear elasticity. **J. Comput. Appl. Math., 236** (2011), 834-842.

[22] Lian, Y., Li, Z., A numerical study on cavitations in nonlinear elasticity-defects and configurational forces. **Math Models Methods Appl. Sci., 21** (2011), 2551-2574.

[23] Lian, Y., Li, Z., Position and size effects on voids growth in nonlinear elasticity. **Int. J. Fract., 173** (2012), 147-161.

[24] Meyer, P. A., Probability and potentials, Blaisdell (1966).

[25] Michel, J., Lopez-Pamies, O., Ponte Castañeda, P., Triantafyllidis, N., Microscopic and macroscopic instabilities in finitely strained fiber-reinforced elastomers. **J. Mech. Phys. Solids, 58(11)** (2010), 1776-1803.

[26] Morrey, C. B., Multiple integrals in the calculus of variations. Springer(1966).

[27] Müller, S., Spector, S. J., An existence theory for nonlinear elasticity that allows for cavitation, **Arch. Rat. Mech. Anal., 131** (1995), 1-66.

[28] Negrón-Marrero, P. V., Betancourt, O., The numerical computation of singular minimizers in two-dimensional elasticity. **J. Comput. Phys., 113** (1994), 291-303.

[29] Sivaloganathan, J., Uniqueness of regular and singular equilibia for spherically symmetric problems of nonlinear elasticity. **Arch. Rat. Mech. Anal., 96** (1986), 97-136.

[30] Sivaloganathan, J., Spector, S. J., On the existence of minimizers with prescribed singular points in nonlinear elasticity. **J. Elast., 59** (2000), 83-113.

[31] Sivaloganathan, J. and Spector, S. J., On cavitation, configurational forces and implications for fracture in a nonlinearly elastic material, **J. Elast., 67** (2002), 25-49.

[32] Sivaloganathan, J., Spector, S. J., Tilakraj, V., The convergence of regularized minimizers for cavitation problems in nonlinear elasticity. **SIAM J. Appl. Math., 66** (2006), 736-757.

[33] Su, C., Li, Z., Orientation-preservation conditions on an Iso-parametric FEM in cavitation computation. Preprint.

[34] Su, C., Li, Z., Error analysis of a Dual-parametric Bi-quadratic FEM in cavitation computation in elasticity. **SIAM J. Numer. Anal., 53(3)** (2015), 1629-1649.

[35] Xu, X., Henao, D., An efficient numerical method for cavitation in nonlinear elasticity. **Math Models Methods Appl. Sci., 21** (2011), 1733-1760.